



Synthesis of porous nano/micro structured LiFePO_4/C cathode materials for lithium-ion batteries by spray-drying method

Xiao-mei GUAN^{1,2}, Guo-jun LI^{1,2}, Chun-yang LI¹, Rui-ming REN¹

1. Liaoning Key Laboratory for New Energy Battery, Dalian Jiaotong University, Dalian 116028, China;
2. School of Materials Science and Engineering, Dalian Jiaotong University, Dalian 116028, China

Received 10 November 2015; accepted 24 May 2016

Abstract: In order to enhance electrochemical properties of LiFePO_4 (LFP) cathode materials, spherical porous nano/micro structured LFP/C cathode materials were synthesized by spray drying, followed by calcination. The results show that the spherical precursors with the sizes of 0.5–5 μm can be completely converted to LFP/C when the calcination temperature is higher than 500 $^\circ\text{C}$. The LFP/C microspheres obtained at calcination temperature of 700 $^\circ\text{C}$ are composed of numerous particles with sizes of ~ 20 nm, and have well-developed interconnected pore structure and large specific surface area of 28.77 m^2/g . The specific discharge capacities of the LFP/C obtained at 700 $^\circ\text{C}$ are 162.43, 154.35 and 144.03 $\text{mA}\cdot\text{h/g}$ at 0.5C, 1C and 2C, respectively. Meanwhile, the capacity retentions can reach up to 100% after 50 cycles. The improved electrochemical properties of the materials are ascribed to a small Li^+ diffusion resistance and special structure of LFP/C microspheres.

Key words: LiFePO_4/C cathode; nano/micro structure; porous material; spray drying; electrochemical properties

1 Introduction

Olivine-structure lithium iron phosphate (LFP) has elicited much attention since its discovery in 1997 [1] because of its low cost, high energy density, safety, structure stability and environmental benignity [2,3]. However, two intrinsic drawbacks of LFP, namely, poor electronic conductivity ($\sim 10^{-11}$ S/cm) and lithium ion diffusion coefficient ($\sim 1.8 \times 10^{-14}$ cm^2/s) at room temperature [4], limit its commercial application. Considerable measures, such as conductive-layer coating [4,5], polyvalent cation doping [6,7] and size reduction [8,9] have been implemented to overcome these drawbacks. Well-dispersed carbon can provide pathways for the transport of electrons, and reductive carbon can avoid the formation of Fe^{3+} [4,10]. Nanoparticles can provide an increased number of surface reaction sites for lithium ions and shorten the diffusion length of lithium ions [11]. However, nano-sized particles aggregate and absorb moisture from air. Technically, micro-sized spherical particles containing clusters of nanoparticles can address the drawbacks of nanoparticles, and spherical particles have better fluidity and higher packing density than the irregular-shaped

powders [12]. Simultaneously, porous strategy allows for the efficient percolation of electrolytes through the electrode, enhancing the diffusion of Li^+ between the active materials [4]. Based on the above facts, LFP/C microspheres composed of interconnected pores and nanoparticles with a homogeneous carbon coating are believed to be an optimized structure and are expected to possess excellent electrochemical properties.

In this work, the spray drying method was employed to prepare spherical precursor as this method is a facile and scalable technique to fabricate micro-sized spherical materials. It was reported that the spherical LFP materials were synthesized by spray drying method in many researches [13–15]. Final LFP/C composites consisting of nanoparticles and interconnected pores were obtained by calcining precursor at different temperatures for 4 h. The structure, morphology and electrochemical performance of LFP/C materials were characterized and tested.

2 Experimental

2.1 Synthesis

A mixture of the as-synthesized $\text{FePO}_4 \cdot 2\text{H}_2\text{O}$, $\text{LiOH} \cdot \text{H}_2\text{O}$ (AR), citric acid (AR), oxalic acid (AR) and

de-ionized water was ball-milled for 15 h to obtain a precursor slurry. The molar ratios of both $\text{FePO}_4 \cdot 2\text{H}_2\text{O}$ to $\text{LiOH} \cdot \text{H}_2\text{O}$ and citric acid to oxalic acid were 1:1. Citric acid and oxalic acid were used as chelating agent, reductant and carbon source. To obtain spray-dried solution, the slurry was placed in an air-circulating oven at 45 °C for 48 h and then diluted to a solution with a mass fraction of 10%. After being stirred at room temperature for 3 h by magnetic stirrers, the solution was spray-dried at 140 °C and 70 °C (inlet and outlet temperatures, respectively) at a feed rate of 450 mL/h to obtain the precursor (light yellow precipitate). During the spray drying step, the feeding spray solution was pumped to a tank reactor with a stream of hot air and sprayed into aerosol. The precursor powder formed as the moisture evaporated rapidly. The dry powder was finally separated from moist air in a centrifugal atomizer and was collected in a vial. Lastly, the precursor was calcined at different temperatures in pure Ar atmosphere. LFP/C composites were obtained as the temperature decreased.

2.2 Characterization

TG–DSC measurement was carried out with a STA904 apparatus from room temperature to 800 °C in Ar atmosphere at a heating rate of 1/6 °C/min. X-ray diffraction (XRD, D/Max-Ultima⁺) was performed with an Empyrean X-ray diffractometer with $\text{Cu K}\alpha$ radiation ($V=40$ kV, $I=40$ mA) to identify the crystalline phase of all samples. The scanning range was from 10° to 90° with a step size of 0.02°. The micro-morphology and particle size of the samples were investigated through scanning electron microscopy (SEM, JEOL/JSM–6360LV). Field emission SEM (FE-SEM, SUPRA 55) was applied to obtaining cross-sectional images of the microspheres. Nitrogen adsorption–desorption isotherm was measured at 77 K after degassing the samples at 125 °C for 4 h, and the tests were conducted with a specific-surface-area analyzer (3SI-MP–11) through Brunauer–Emmett–Teller (BET) and Barrett–Joyner–Halenda (BJH) methods.

2.3 Electrochemical measurements

The electrochemical properties of the as-prepared LFP/C powders as active cathode materials were evaluated by using a two-electrode coin-type cell (CR2032) of $\text{Li}|\text{LiPF}_6|\text{LFP/C}$ ($V(\text{EC}):V(\text{EMC}):V(\text{DMC})=1:1:1$). The separator was a polypropylene membrane (Celgard 2400), and the lithium metal served as the counter and reference electrode. The working cathode slurry was fabricated by mixing the active material (LFP/C), super P II and polyvinylidene fluoride (PVDF) at a mass ratio of 80:7:13 in *N*-methyl pyrrolidinone (NMP). The slurry was prepared as follows: PVDF (13%, mass fraction) was dissolved in NMP to obtain a uniform,

transparent and viscous liquid. Then, the LFP/C (80%, mass fraction) and super P II (7%, mass fraction) were added into the solution in turn. The suspension was stirred for 6–8 h to obtain uniform slurry. The slurry was pasted onto an Al foil with a thickness of 50 μm and dried at 70 °C for 4 h in an oven and 110 °C for 12 h in vacuum. After cooling to room temperature, the Al foil with active material was punched into disks with 10 mm in diameter. LFP/C was approximately 4.0 mg in each disk.

The cells were assembled in a glove box (Unilab, MB–20–G) filled with dry and high-purity Ar gas. Galvanostatic charge–discharge tests at different current densities with voltages ranging from 2.0 to 4.2 V were performed on a Neware battery tester. A cyclic voltammetry (CV) test was conducted on an electrochemical workstation (CHI660B, CH Instruments) in a voltage range of 2.5 to 4.2 V and at a scan rate of 0.1 mV/s. Electrochemical impedance spectroscopy (EIS) was also conducted on an electrochemical workstation (AUTOLAB, PGSTAT302N) in a frequency range of 100000–0.01 Hz. All tests were performed at room temperature.

3 Results and discussion

3.1 Phase composition

Figure 1 shows the TG and DSC curves of the precursor. The TG curve presents several mass losses and the DSC curve displays the corresponding endothermic or exothermic peaks. The first mass loss (about 13%) from room temperature to 170 °C is caused by the release of physically absorbed water and crystal water of citrate [16]. The second mass loss corresponding to the endothermic peaks at approximately 180 °C results from the dehydration of oxalate [17]. The next mass loss accompanied by the endothermic peak from 225 to 300 °C is attributed to the decomposition of citrate [16]. The weak endothermic peak between 300 and 400 °C is due to the decomposition of oxalate into amorphous

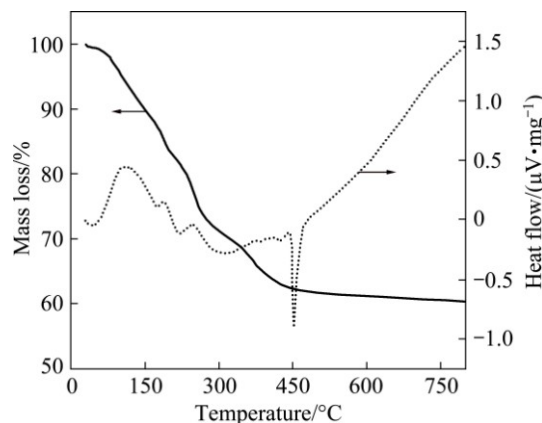


Fig. 1 TG–DSC curves of precursor

carbon, CO_2 and CO [17] with the synthesis of $\text{Li}_3\text{Fe}_2(\text{PO}_4)_3$ and Fe_2O_3 , as shown in Fig. 2(b). The last two exothermic peaks, approximately 10%, coincide with the last mass loss between 300 °C and 500 °C. The weak exothermic peak at about 440 °C can be explained by the reduction of Fe_2O_3 to FeO . The last and obvious exothermic peak at 450 °C stands for the synthesis of LFP/C by solid state reaction of $\text{Li}_3\text{Fe}_2(\text{PO}_4)_3$, FeO and C . No mass loss was observed above 500 °C, meaning that the precursor can be completely converted to LFP when the temperature is more than 500 °C.

Figure 2 shows the XRD patterns of the samples obtained at different temperatures. It is seen from Fig. 2(a) that the spray-dried precursor has no diffraction peaks, suggesting that it is amorphous. The products obtained at 350 °C are Fe_2O_3 and $\text{Li}_3\text{Fe}_2(\text{PO}_4)_3$ with poor crystallinity. When the temperature rises to 450 °C, LFP diffraction peaks are detected. When the temperature is more than 550 °C, the XRD patterns of the obtained samples are in good accordance with the standard LFP card (JPDF No. 81–1173) indexed by orthorhombic olivine-type structure (space group $p\text{mnb}$), which shows that the amorphous precursor can be completely converted to LFP. The XRD results are in agreement

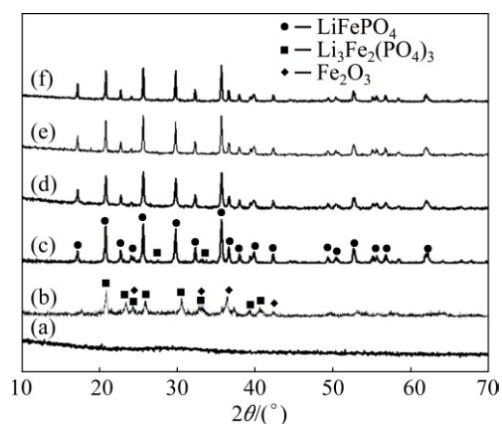


Fig. 2 XRD patterns of samples obtained at different temperatures: (a) Precursor; (b) 350 °C; (c) 450 °C; (d) 550 °C; (e) 700 °C; (f) 800 °C

with the TG–DSC curves shown in Fig. 1. No typical diffraction peaks of carbon are found, indicating that coating carbon exists in an amorphous form.

3.2 Particle morphology

Figure 3 shows the SEM images of the spray-dried precursor and as-prepared samples at different

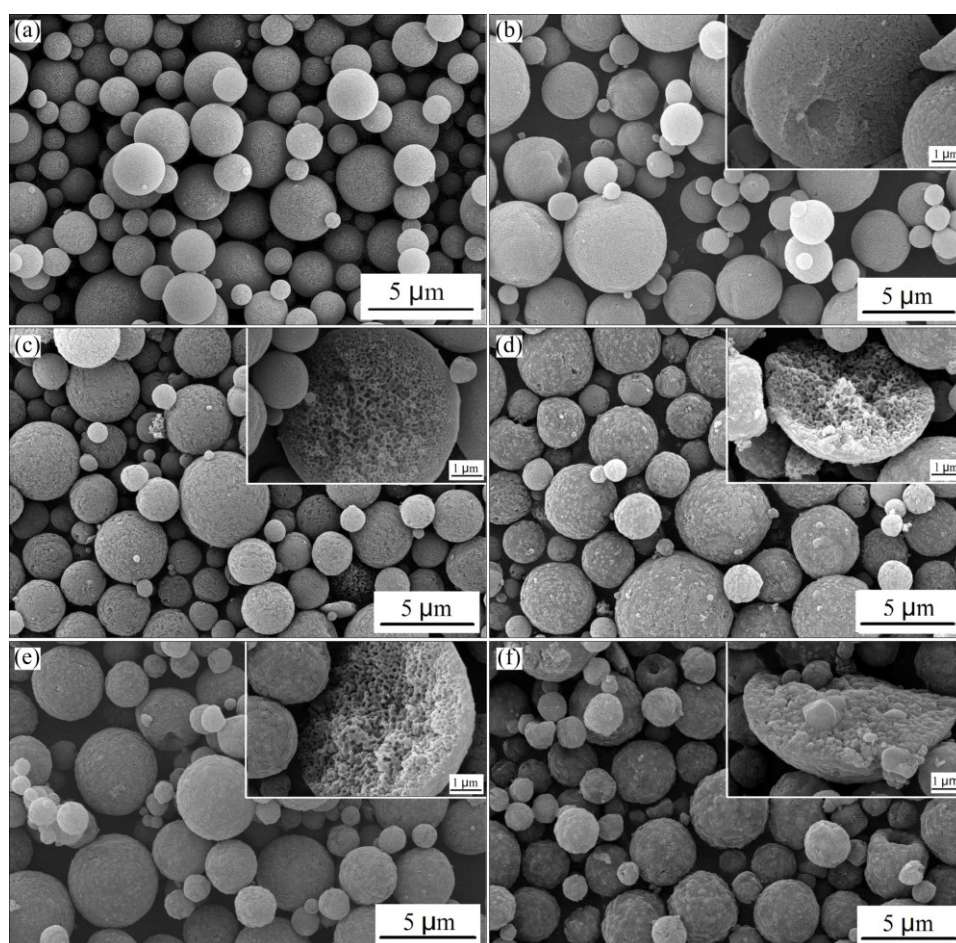


Fig. 3 SEM images of samples obtained at different temperatures: (a) Spray-dried precursor; (b) 550 °C; (c) 650 °C; (d) 700 °C; (e) 750 °C; (f) 800 °C

temperatures. As shown in Fig. 3(a), the precursor particles are spherical with a large diameter range of 0.5–5 μm , which can be contributed to high tap density owing to the fact that spherical particles with large size range can be packed closely and easily [16,17]. After calcination at different temperatures for 4 h, the spherical morphology is preserved and the as-prepared LFP/C microspheres are composed of nanoparticles and interconnected pores, as shown in Figs. 3(b)–(e). When the calcination temperature is 550 $^{\circ}\text{C}$, the particles are solid and less pores exist on the surfaces or inside the microspheres. The surfaces of the microspheres obtained at 650 $^{\circ}\text{C}$ are rough and have open pores, and the interconnected pores inside particles also increase, as shown in Fig. 3(c). The as-prepared LFP/C samples at 700 and 750 $^{\circ}\text{C}$ have good developed interconnect-pore structures. Nanoparticles grow up gradually along with further increasing the calcination temperature, reducing the quantity of pores on the surfaces and within the microspheres. After calcination at 800 $^{\circ}\text{C}$, nanoparticles on the surfaces aggregate together and the interconnected pores are fully filled with the grown nanoparticles, which can be seen from Fig. 3(f). The interconnected pores can enhance the infiltration of liquid electrolyte to the electrode materials and increase the transport rate of Li^+ in the microspheres. Given the fact that practical performance of materials depends on their microstructures, LFP/C samples obtained at 650, 700 and 750 $^{\circ}\text{C}$ with good porous structures are expected to exhibit good electrochemical performance.

The N_2 adsorption and desorption isotherms (BJH and BET) of LFP/C samples obtained at 650, 700 and 750 $^{\circ}\text{C}$ were tested to obtain further information of the porous structure, and the results are shown in Fig. 4. The pore size distribution curves reveal that interconnected pores exist in all three samples (size distribution range of 3 to 30 nm). The microspheres obtained at 700 $^{\circ}\text{C}$ have a better-developed pore strategy than microspheres obtained at 650 and 750 $^{\circ}\text{C}$. During calcination, oxalate and citrate go through a process of melting, polymerization decomposition and carbonization, generating gaseous products, such as water vapor, CO_2 and CO , which are responsible for the formation of a porous structure. Figure 4(b) shows type-IV isotherms according to the International Union of Pure and Applied Chemistry classification, suggesting the porous nature of the materials [18]. The specific surface area of the prepared LFP/C at 700 $^{\circ}\text{C}$ is 28.77 m^2/g , larger than those of the other two samples obtained at 650 $^{\circ}\text{C}$ (26.12 m^2/g) or 750 $^{\circ}\text{C}$ (23.89 m^2/g). A large specific surface area can facilitate the insertion and desertion of lithium ions and the transport of electrons, which can in turn alleviate electrode polarization to some extent [4]. In sum, 700 $^{\circ}\text{C}$ was selected as the ideal calcination

temperature.

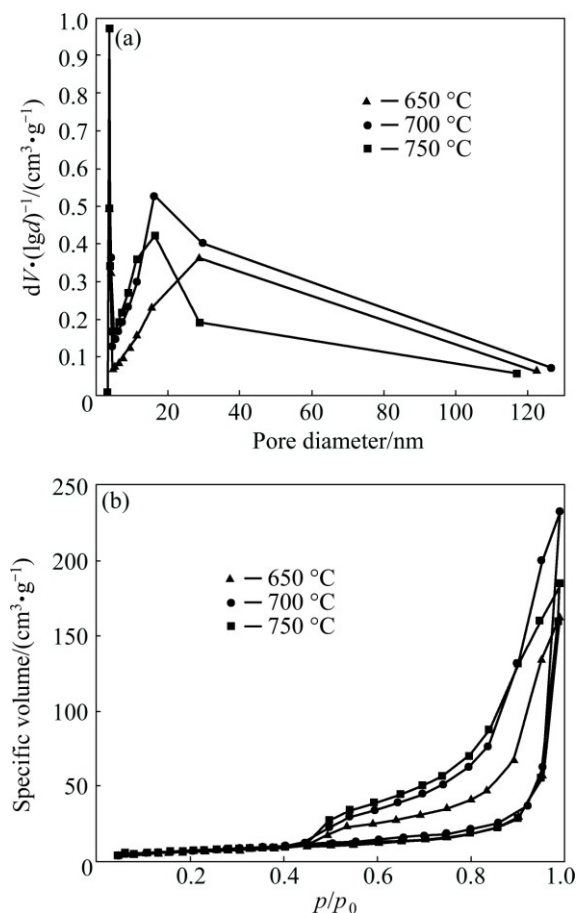


Fig. 4 N_2 adsorption and desorption isotherms of LFP/C samples obtained at 650, 700 and 750 $^{\circ}\text{C}$: (a) Pore size distribution (BJH); (b) Specific volume of pore under relative pressure for specific surface area

Figure 5 shows the cross-sectional FE-SEM images of a single LFP/C microsphere obtained at 700 $^{\circ}\text{C}$ and different magnifications. The microspheres are composed of primary nanoparticles with a size of approximately 20 nm, and the interconnected pores distribute uniformly around the primary nanoparticles. Theoretically, a small particle size means small diffusion length and large surface reaction sites for lithium ion, which can improve the lithium-ion intercalation kinetics and even the electrochemical performance of materials [19].

3.3 Electrochemical performance

Figures 6(a) and (b) show the EIS curves of samples obtained at 650, 700 and 750 $^{\circ}\text{C}$ and the cyclic voltammetry profile of the LFP/C sample obtained at 700 $^{\circ}\text{C}$, respectively. Figure 6(c) shows the equivalent circuit of EIS test and the fitting plot of the equivalent circuit of the obtained LFP/C at 700 $^{\circ}\text{C}$. By comparison, the fitting plot is similar to the EIS curves shown in Fig. 6(a), consisting of a semicircle in the high-to-medium frequency region and an inclined line in the

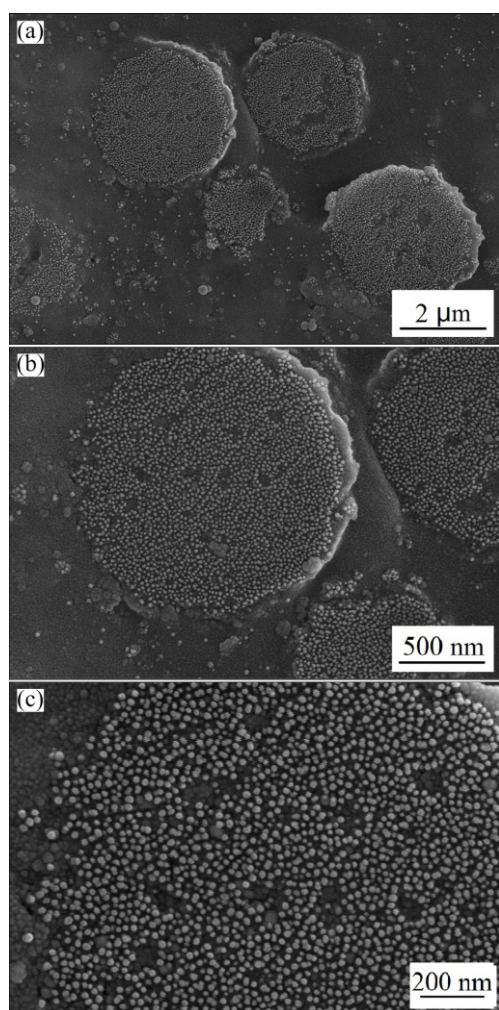


Fig. 5 Cross-sectional FE-SEM images of LFP/C particles obtained at 700 °C

low-frequency region. The intercept on the Z' axis in the high-frequency region refers to ohmic resistance (R_s) of the electrolyte. Based on the test, R_s values of the samples obtained at 650, 700 and 750 °C are 2.03, 1.06 and 1.60 Ω , respectively. With regard to the charge transfer resistance (R_{ct}), corresponding to the semicircle in EIS curve, the EIS curves also display a tendency of LFP/C (700 °C) < LFP/C (750 °C) < LFP/C (650 °C). R_{ct} is related to a complex reaction of charge transfer process between the electrolyte and the active materials [20,21]. The sloping line in the low-frequency region means the Warburg impedance (Z_w). Z_w results from the diffusion of the lithium ion in the bulk of electrode materials [22,23]. By comparison, the slope of the inclined line of the sample obtained at 700 °C in the low-frequency region is larger than that of the other samples, meaning a faster lithium-ion diffusion rate. The constant phase CPE in simplified equivalent circuit model is placed to represent the double layer capacitance and passivation film capacitance, and the capacitance resistances are too

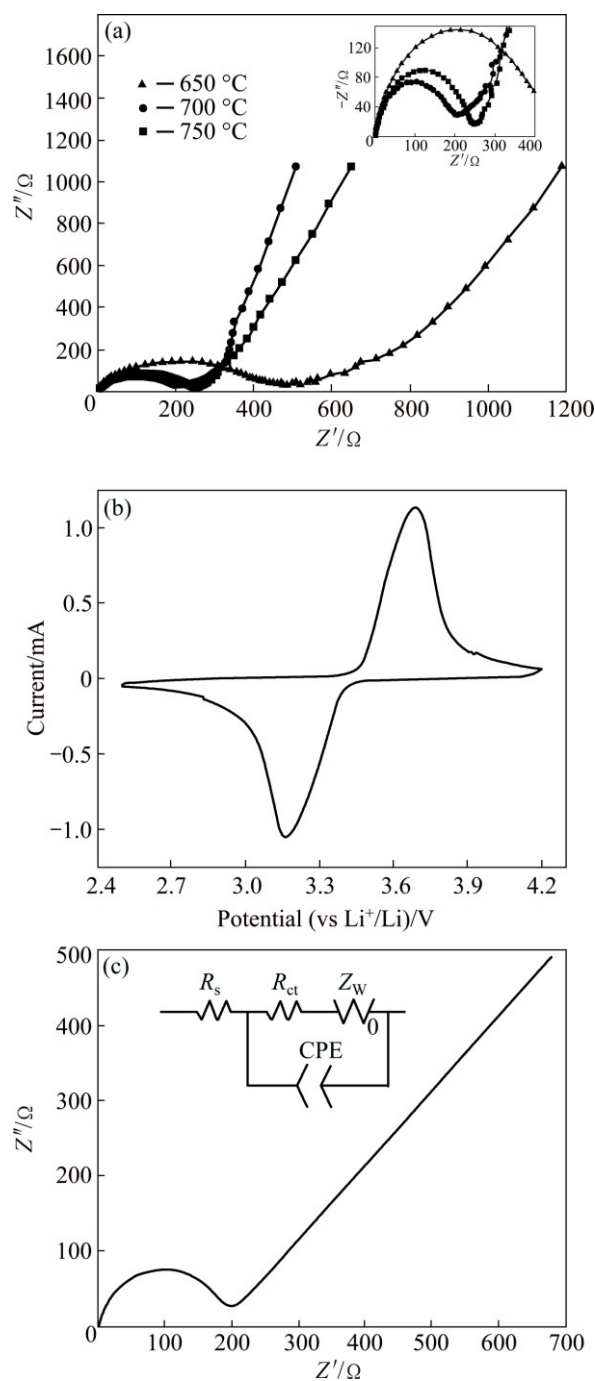


Fig. 6 EIS curves of samples obtained at different temperatures (a), cyclic voltammetry profile of LFP/C sample obtained at 700 °C (b) and equivalent circuit of EIS test and fitting plot (c)

small to be negligible [24]. According to the analyses above, the sample obtained at 700 °C has smaller ohmic impedance, charge transfer impedance and Warburg impedance. Combining the large specific surface area and small impedances, the sample obtained at 700 °C should have better electrochemical performances than the other two samples.

The CV curve shown in Fig. 6(b) shows that the electrodes of this sample have a couple of anodic and

cathodic peaks, corresponding to the two-phase reaction based on the redox couple of $\text{Fe}^{2+}/\text{Fe}^{3+}$ during lithium ion extraction and insertion process in olivine LFP. The approximately symmetrical redox peaks can be ascribed to the rapid ion-exchange and suggest a good charge–discharge reversibility of the as-prepared LFP/C active material, theoretically [22].

The initial specific charge–discharge capacities and cycling performance of the LFP/C sample obtained at 700 °C and different current rates are shown in Fig. 7. The specific discharge capacity at 0.5C (85 mA/g) can reach up to 162.43 mA·h/g, corresponding to 95.3% of the theoretical capacity (170 mA·h/g), better than most of similar investigations [3,13]. As the current rates change to 1C and 2C, the initial discharge capacities are 154.35 and 144.03 mA·h/g, respectively. The discharge capability at high current rates heavily depends on the fast transference of electrons between particles [25]. Because of the short Li^+ diffusion path, low charge transfer resistance and high reaction kinetics [26,27], the polarization potentials are 0.17, 0.26 and 0.48 V at 0.5C, 1C and 2C, respectively. The specific capacity retentions are nearly 100% after 50 cycles, as shown in Fig. 7(b). This result indicates that the prepared LFP/C shares good

conductive ability and cycling stability. The fluctuations within a narrow range are contributed to the electrolyte decomposition with increasing temperature during the prolonged cycle process. The high specific capacities and good cycling stability are attributed to the special porous nano/micro structure of the microspheres and the small Li^+ diffusion resistance.

4 Conclusions

1) The results of the XRD and SEM indicate the amorphous precursors are microspheres with a size range of 0.5 to 5 μm and can be completely converted to LFP/C when temperature is more than 500 °C. The final LFP/C microspheres are composed of nanoparticles and interconnected pores.

2) The nanoparticle size of the LFP/C sample obtained at 700 °C is about 20 nm. LFP/C cathode material obtained at this temperature has a large specific surface area of 28.77 m^2/g , small impedance and fast Li^+ diffusion rate. The initial specific discharge capacities of LFP/C composites are 162.43, 154.35 and 144.03 mA·h/g at 0.5C, 1C and 2C, respectively. After 50 cycles, the retentions of capacities can reach up to 100%. The enhanced electrochemical properties can be ascribed to the unique porous nano/micro structure and a the small Li^+ diffusion resistance of the as-prepared LFP/C material.

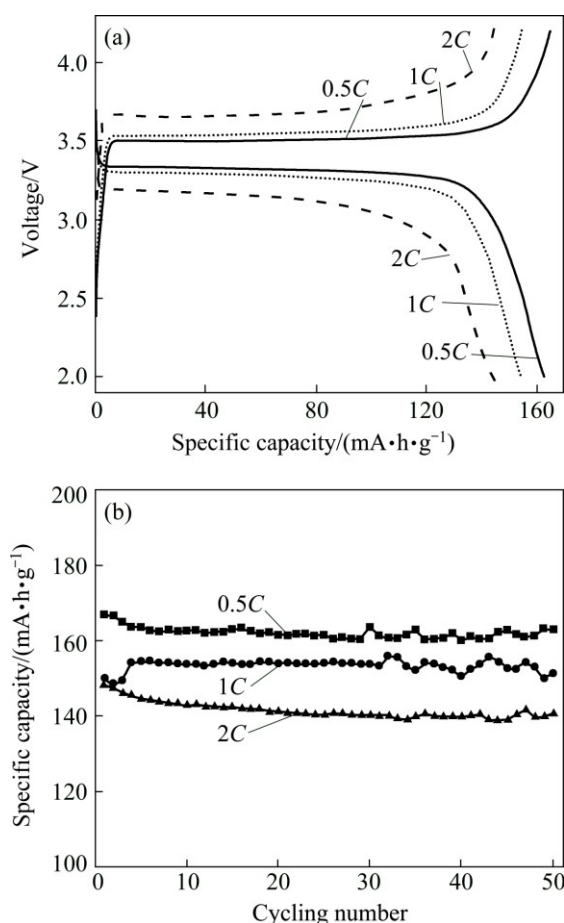


Fig. 7 Initial charge–discharge curves (a) and cycling performance (b) of LFP/C sample obtained at 700 °C and different current rates

References

- [1] PADHI A K, NANJUNDASWAMY K S, GOODENOUGH J B. Phospho-olivines as positive-electrode materials for rechargeable lithium batteries [J]. *Electrochemical Society*, 1977, 144: 1188–1194.
- [2] JU Shi-yuan, PENG Hong-ru, LI Gui-cun, CHEN Ke-zheng. Synthesis and electrochemical properties of LiFePO_4 single-crystalline nanoplates dominated with bc-planes [J]. *Material Letters*, 2012, 74: 22–25.
- [3] ZOU Bing-fang, WANG Yong-qiang, ZHOU Shao-min. Spray drying-assisted synthesis of LiFePO_4/C composites microspheres with high performance for lithium-ion batteries [J]. *Materials Letters*, 2013, 92: 300–303.
- [4] MI Ying-ying, GAO Ping, LIU Wen, ZHANG Wei-dong, ZHOU Heng-hui. Carbon nanotube-loaded mesoporous $\text{LiFe}_{0.6}\text{Mn}_{0.4}\text{PO}_4/\text{C}$ microspheres as high performance cathodes for lithium-ion batteries [J]. *Journal of Power Sources*, 2014, 267: 450–468.
- [5] SONG Hai-shen, CAO Zheng, ZHANG Zhi-an, LAI Yan-qing, LI Jie, LIU Ye-xiang. Effect of vinylene carbonate as electrolyte additive on cycling performance of $\text{LiFePO}_4/\text{graphite}$ at elevated temperature [J]. *Transaction of Nonferrous Metals Society of China*, 2014, 24: 723–718.
- [6] CHUNG S Y, BLOKING J K, CHIANG Y M. Electronically conductive phospho-olivines as lithium storage electrodes [J]. *Nature Materials*, 2002, 1: 123–128.
- [7] TANG Hao, TAN Long, XU Jun. Synthesis and characterization of LiFePO_4 coating with aluminum doped zinc oxide [J]. *Transaction of Nonferrous Metals Society of China*, 2013, 23: 451–455.
- [8] KNAG B, CEDER G. Battery materials for ultrafast charging and

- discharging [J]. Nature, 2009, 458: 190–193.
- [9] HUANG Yang-hui, REN Hai-bo, YIN Sheng-yu, WANG Yun-hong, PENG Zheng-he, ZHOU Yun-hong. Synthesis of LiFePO_4/C composite with high-rate performance by starch sol assisted rheological phase method [J]. Journal of Power Sources, 2010, 195: 610–613.
- [10] HUI Bi, HUANG Fu-qiang, TANG Yu-feng, LIU Zhan-qiang, LIN Tian-quan, CHEN Jian, ZHAO Wei. Study of LiFePO_4 cathode modified by grapheme sheets for high-performance lithium ion batteries [J]. Electrochimica Acta, 2013, 88: 414–420.
- [11] DU Juan, JIAO Li-fang, WU Qiang, LIU Yang-chang, GUO Li-jing, WANG Yi-jing, YUAN Hua-tang. Mesoporous LiFePO_4 microspheres for rechargeable lithium-ion batteries [J]. Electrochimica Acta, 2013, 98: 288–293.
- [12] HUANG Bi, ZHENG Xiao-dong, FAN Xiao-ping, SONG Guan-hui, LU Mi. Enhanced rate performance of nano-micro structured LiFePO_4/C by improved process for high-power Li-ion batteries [J]. Electrochimica Acta, 2011, 56: 4865–4868.
- [13] WU Ling, ZHONG Sheng-kui, LIU Jie-qun, LV Fang, WAN Fang. High tap-density and high performance LiFePO_4/C cathode material synthesized by the combined sol spray-drying and liquid nitrogen quenching method [J]. Materials Letters, 2012, 89: 32–35.
- [14] SHU Hong-bo, CHEN Man-fang, FU Yan-qing, YANG Xiu-kang, YI Xin, BAI Yan-song, LIANG Qian-qian, WEI Qi-liang, HU Be-nan, TAN Jin-li, WU Chun, ZHOU Meng, WANG Xian-you. Improvement of electrochemical performance for spherical LiFePO_4 via hybrid coated with electron conductive carbon and fast Li ion conductive $\text{La}_{0.56}\text{Li}_{0.33}\text{TiO}_3$ [J]. Journal of Power Sources, 2014, 252: 73–78.
- [15] CHEN Man-fang, WANG Xian-yang, SHU Hong-bo, YU Rui-zhi, YANG Xiu-kang, HUANG Wei-hua. Solvothermal synthesis of monodisperse micro-nanostructure starfish-like porous LiFePO_4 as cathode material for lithium-ion batteries [J]. Journal of Alloys and Compounds, 2015, 652: 213–219.
- [16] XIN Xin-quan, WANG Xin, ZHANG Xue-qin, DAI An-bang. Studies on thermal stabilities of coordination compounds by gas chromatography [J]. Acta Chimica Sinica, 1982, 40: 1112–1122. (in Chinese)
- [17] ZHOU Shun, XU Ying-bo, WANG Chen-hui, TIAN Zhen-feng. Pyrolytic behavior of citric acid [J]. Tobacco Chemistry, 2011, 9: 45–49. (in Chinese)
- [18] LI Min, HOU Xian-hua, SHA Yu-jing, WANG Jie, HU She-jun, LIU Xiang. Facile spray-drying/pyrolysis synthesis of core-shell structure graphite/silicon-porous carbon composites as a superior anode for Li-ion batteries [J]. Journal of Power Sources, 2014, 248: 721–728.
- [19] WEN Si-jing, LI Guo-jun, REN Rui-ming, LI Chun-yang. Preparation of spherical $\text{Li}_4\text{Ti}_5\text{O}_{12}$ anode materials by spray drying [J]. Material Letters, 2015, 148: 130–133.
- [20] MA Zhi-ping, FAN Yu-quan, SHAO Guang-jie, LIN Wang, SONG Jian-juan. Cupric ion substituted LiFePO_4/C composites with enhanced electrochemical performance for Li-ion batteries [J]. Electrochimica Acta, 2014, 139: 256–263.
- [21] ZHUANG Quan-chao, QIU Xiao-yun, XU Shou-dong, QIANG Ying-huan, SUN Shi-guang. Diagnosis of electrochemical impedance spectroscopy in lithium ion batteries [C]//Lithium Ion Batteries–New Developments. Xiamen: INTECH Open Access Publisher, 2012.
- [22] SU Chang, BU Xi-dan, XU Li-huan, LIU Jun-lei, ZHANG Chen. A novel $\text{LiFePO}_4/\text{graphene}/\text{carbon}$ composite as a performance-improved cathode material for lithium-ion batteries [J]. Electrochim Acta, 2012, 64: 190–195.
- [23] THORAT I V, MATHUR V, HARB J N, WHER D R. Performance of carbon-fiber-containing LiFePO_4 cathodes for high-power applications [J]. Journal of Power Sources, 2006, 162: 673–678.
- [24] WANG G X, YANG L, CHEN Y, WANG J Z, BEWLEY S, LIU H K. An investigation of polypyrrole– LiFePO_4 composite cathode materials for lithium-ion batteries [J]. Electrochimica Acta, 2005, 50: 4649–4654.
- [25] THOART I V, JOSHI T, ZAGHBI K, HARB J N, WHEELER D R. Understanding rate-limiting mechanisms in LiFePO_4 cathodes for Li-ion batteries [J]. Electrochemical Society A, 2011, 158: 1185–1193.
- [26] SHU Hong-bo, WANG Xian-you, WU Qiang, HU Be-nan, YANG Xiu-kang, WEI Qi-liang, LIANG Qian-qian, BAI Yan-song, ZHOU Meng, WU Chun, CHEN Man-fang, WANG Ai-wen, Jiang Lan-lan. Improved electrochemical performance of LiFePO_4/C cathode via Ni and Mn co-doping for lithium-ion batteries [J]. Journal of Power Sources, 2013, 237: 149–155.
- [27] HSIEH C T, CHEN I L, CHEN W Y, WANG J P. Synthesis of iron phosphate powders by chemical precipitation route for high-power lithium iron phosphate cathodes [J]. Electrochimica Acta, 2012, 83: 202–208.

喷雾干燥法合成纳微多孔球形 LiFePO_4/C 锂离子电池正极材料

管晓梅^{1,2}, 李国军^{1,2}, 黎春阳¹, 任瑞铭¹

1. 大连交通大学 辽宁省新能源电池重点实验室, 大连 116028;

2. 大连交通大学 材料科学与工程学院, 大连 116028

摘要: 为提高 $\text{LiFePO}_4(\text{LFP})$ 正极材料的电化学性能, 采用喷雾干燥结合煅烧工艺合成具有纳微结构和多孔结构的球形 LFP/C 材料。结果表明, 当煅烧温度高于 $500\text{ }^\circ\text{C}$ 时, 粒径尺寸为 $0.5\sim 5\text{ }\mu\text{m}$ 的球形前驱体可以完全转化为 LFP/C 材料。当煅烧温度为 $700\text{ }^\circ\text{C}$ 时, 所得的 LFP/C 微米球形颗粒是由大量粒径约为 20 nm 的颗粒及发育良好且相互连通的孔道组成, 其比表面积为 $28.77\text{ m}^2/\text{g}$ 。在 0.5C 、 1C 和 2C 的电流倍率下恒流充放电时, $700\text{ }^\circ\text{C}$ 时所得 LFP/C 材料的放电比容量分别为 162.43 、 154.35 和 $144.03\text{ mA}\cdot\text{h/g}$, 且 50 次循环后的容量保持率达到 100% 。该材料所具有良好的电化学性能得益于其较小的 Li^+ 扩散阻抗和特殊的微观结构。

关键词: LiFePO_4/C 正极材料; 纳-微结构; 多孔材料; 喷雾干燥; 电化学性能

(Edited by Wei-ping CHEN)